Received: 25 March 2020 | Revised: 29 May 2020 | Accepted: 2 July 2020

DOI: 10.4218/etrij.2020-0116

SPECIAL ISSUE

ETRI Journal WILEY

An impulse radio (IR) radar SoC for through-the-wall human-detection applications

Piljae Park | **Sungdo Kim** | **Bontae Koo**

AI Compact SoC Research Section, Electronics and Telecommunications Research Institute, Daejoen, Republic of Korea

Correspondence
Piljae Park, AI Compact SoC Research Section, Electronics and Telecommunications Research Institute, Daejone, Republic of Korea.
Email: nahoona@gmail.com

Funding information
This research was supported by the IITP 2019-0-00006, KEIT 10067194.

More than 42 000 fires occur nationwide and cause over 2500 casualties every year. There is a lack of specialized equipment, and rescue operations are conducted with a minimal number of apparatuses. Through-the-wall radars (TTWRs) can improve the rescue efficiency, particularly under limited visibility due to smoke, walls, and collapsed debris. To overcome detection challenges and maintain a small-form factor, a TTWR system-on-chip (SoC) and its architecture have been proposed. Additive reception based on coherent clocks and reconfigurability can fulfill the TTWR demands. A clock-based single-chip infrared radar transceiver with embedded control logic is implemented using a 130-nm complementary metal oxide semiconductor. Clock signals drive the radar operation. Signal-to-noise ratio enhancements are achieved using the repetitive coherent clock schemes. The hand-held prototype radar that uses the TTWR SoC operates in real time, allowing seamless data capture, processing, and display of the target information. The prototype is tested under various pseudo-disaster conditions. The test standards and methods, developed along with the system, are also presented.

KEYWORDS
CMOS radar, IR radar, radar transceiver, Through-the-wall radar, UWB radar

1 | INTRODUCTION

Demands for safety against disasters (either natural or man-made) have been increasing. Firefighting infrastructure and personnel play key roles in various disaster scenarios. However, for the rescue operation, specialized equipment is still lacking. Human-detection devices constitute one of the examples that can help overcome adverse conditions.

According to the 2019 Annual Report of the Korean National Fire Agency, more than 42 000 fires occurred nationwide and resulted in more than 2500 casualties in 2018 [1]. Among these cases, rescue operations often require that fire fighters enter the fire scene with minimal rescue-aid devices, such as flash lights and walkie-talkies. In contrast, in military tactical operations, mission-specific devices, such as through-the-wall radars (TTWRs), help operators cope with various situations [2–6]. In the case of firefighters, TTWRs can improve the operation efficiency and reduce risks by identifying the imperiled in invisible conditions. Performance, ruggedness, and usability, including light weight are key requirements. Therefore, system-on-chip (SoC) is a very desirable solution for versatile and small-form factor TTWRs.

Previously, TTWR have been developed mostly for military applications. Table 1 lists the commercial TTWRs and their features [4–6]. The operating frequency can be chosen based upon losses against obstacles, target resolution, and

This is an Open Access article distributed under the term of Korea Open Government License (KOGL) Type 4: Source Indication + Commercial Use Prohibition + Change Prohibition (http://www.kogl.or.kr/info/licenseTypeEn.do).
1225-6463/$ © 2020 ETRI

TABLE 1 Commercial TTWRs and their features [4–6]

Features	Xaver 100	STM DAR	RO 400	TeTWis 4.3	PRISM 200
Modulation	UWB	UWB/SFCW	N/A	UWB SFCW	UWB
Band (GHz)	3–10	1–5	0.2–0.6	1.9–3.6	1.6–2.2
Range (m)[a]	4, 8, 20	12	21	20	N/A
Resolution (cm)	50	7.5	15	N/A	30
Weight (kg)	0.66	7.5	5.5	7.2	5.7
Comments	1D, Handy	2D, Portable	2D, Portable	2D, Portable	2D&3D, Portable

[a]Maximum detectable range (no guarantee for the through-wall operation).

system form factor. In general, a longer wavelength is better for the penetration but requires larger size mainly due to the antenna size. The modulation scheme and the bandwidth determine the target resolution as well as the target identification algorithm. In most systems, the impulse (UWB) scheme is adopted. Compared with continuous wave (CW) modulation, the time-domain wall separation, and the diminished interaction with the front wall are advantages.

SoC radars are beneficial for the TTWRs thanks to its smaller form-factor, reconfigurability. Prior arts on the single chip radar transceivers that integrate the wideband front-end have been reported [7–12]. Infrared (IR) radars have focused on achieving a high-range resolution. Specifically, a 7.3-mm resolution [8] in 30-nm and 1.2-mm resolution [9] in 55 nm technologies have been reported. However, to apply a SoC radar for TTWRs, not only the resolution but also reconfigurability and performance enhancement schemes are needed.

In this study, a single-chip SoC is proposed for the TTWRs and a hand-held TTWR system for the firefighting operation is demonstrated. To achieve through-wall performance, a time-expansion clock technique is utilized and signal-to-noise ratio (SNR) enhancement is achieved. Reconfiguration of the radar modes for the various conditions can facilitate the use of the TTWR. Test sites for the pseudo-disaster conditions and test standards have been codeveloped [16–18]. The prototype hand-held TTWR was tested subject to the facility and test standards. The results confirmed the performances, including through-wall/debris detections in various materials. The major contributions of the work are as follows: first, radar SoC architecture is proposed that is fully controlled with embedded logic and clock schemes. Second, based on the controllability, through-wall operation is demonstrated. To overcome increased losses due to the wall, an SNR enhancement technique is presented that is a direct consequence of the transceiver architecture. Lastly, the SoC is tested in a system which is close to the final product and the tests are conducted in pseudo-disaster environments with a standard protocol.

The study is organized as follows. The radar architecture and its circuit implementations are introduced specifically to overcome the challenges in through-wall operations. The embedded radar control logic and clock generator are discussed. The prototype radar and test environments are described. Finally, the tested results and discussions are summarized.

TABLE 2 Wall penetration losses [13,14]

Materials	4 GHz	10 GHz	24 GHz
Plywood (2 cm)	1 dB	2 dB	3 dB
Pine Board (2 cm)	1 dB	2 dB	4 dB
Clay Brick	2 dB	3 dB	5 dB
Concrete Block	5 dB	13 dB	35 dB
Reinforced Concrete[a]	39 dB	N/A	45 dB

[a]Frequencies at 5.8 GHz, 28 GHz w/33 cm wall [14].

2 | TWR SOC ARCHITECTURE

In this section, the challenges for TTWRs and the requirements of the radar operation are discussed. The radar operation and its architecture are then introduced.

2.1 | Through-the-wall radar operations and the radar link

A TTWR transmits a signal and detects echo signals from targets beyond the wall. Specifically, weak echo signals from the targets owing to the wall loss need to be identified in the presence of a strong blocker, that is, the echo signal from the wall. The wall losses must be quantified first to establish a sufficient through-wall radar link. Table 2 shows the losses of the walls for different materials. Concrete block and reinforced concrete are the most lossy materials. In the radar link equation, the received power and the SNR are:

$$P_{\mathrm{r}} = \frac{P_{\mathrm{t}} \cdot G_{\mathrm{t}} \cdot G_{\mathrm{r}} \cdot \sigma \cdot \lambda^2}{(4\pi)^3 \cdot R^4 \cdot L_{\mathrm{w}}}, \tag{1}$$

$$\mathrm{SNR} = \frac{P_{\mathrm{r}}}{kTB \cdot F_N \cdot L_{\mathrm{w}}}. \tag{2}$$

where P_r is the received power; P_t is the transmit power, G_t, G_r are the transmission and reception antenna gains, respectively, σ is the radar cross-section of the target, λ is the wavelength, R is the radar range, SNR is the output signal-to-noise ratio of the receiver; k is the Boltzmann constant, T is the absolute temperature, F_N is the noise figure of the receiver, and L_w is the wall loss.

Based on the equations, the wall loss decreases the received power and the SNR of the link. For through-wall operations, the radar transceiver needs to maintain the SNR in spite of the loss. The target motions (ie, human) are very slow compared with the radar operation time (ie, PRF-pulse repetition frequency). The received echo signals can add up coherently for many pulse repetition interval (PRI) durations (ie, inverse of PRF). To compensate a concrete block wall loss (ie, ~20 dB for both ways), the radar architecture in this study utilizes the repetitive coherent addition in the reception of the echo pulses.

The second-order effects due to the wall, such as the "blocking zone" emerge especially when the direct wall blocker saturates the radar receiver. The radar control logic seen in Figure 1 can control sensitivity dynamically to mitigate the wall effect. In contrast to the wall-contacting operations that avoid the wall blocker effects, the prototype radar for our work needs to operate from the wall. The prototype radar includes reconfigurability for the range. The wall blocker can be separated from target candidates.

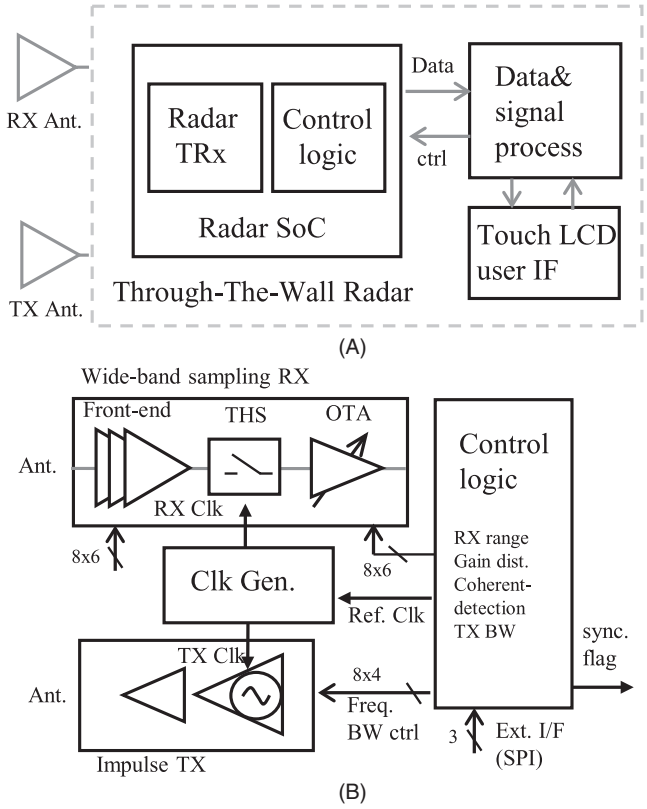

FIGURE 1 (A) Through-the-wall radar system architecture and (B) radar system-on-chip (SoC) block diagram

2.2 | Time-expansion radar

A human target is nearly stationary compared with a single radar operation time (PRI). Multiple pulses can be transmitted for echo pulse recovery. The reconstruction is achieved in a piece-by-piece manner from the multiple received pulses. Therefore, the recovered pulse is observed in an "expanded time" scale. Time-expansion radars that utilize repetitive reception have been demonstrated [7–9]. The principle of the operation is presented in [10]–the Appendix

The IR radar detects its range based upon the time relation between transmit (TX) and receive clock (RX) clocks (CLKs). At the rising edge of the TX clock, the transmitter fires an impulse through the antenna. After a round-trip delay, an echo pulse returns. Figure 2 shows the timing diagram of the clock signals used in the proposed radar. From one TX/RX clock operation (within a PRI seen in Figure 2A), the receiver recovers a single-range point among the full range of points (bins). To recover a different range of points, the TX–RX delay (T_d) needs to change. The delay resolution (δt in Figure 2) determines the range resolution. For full-range recovery, multiple pairs of TX/

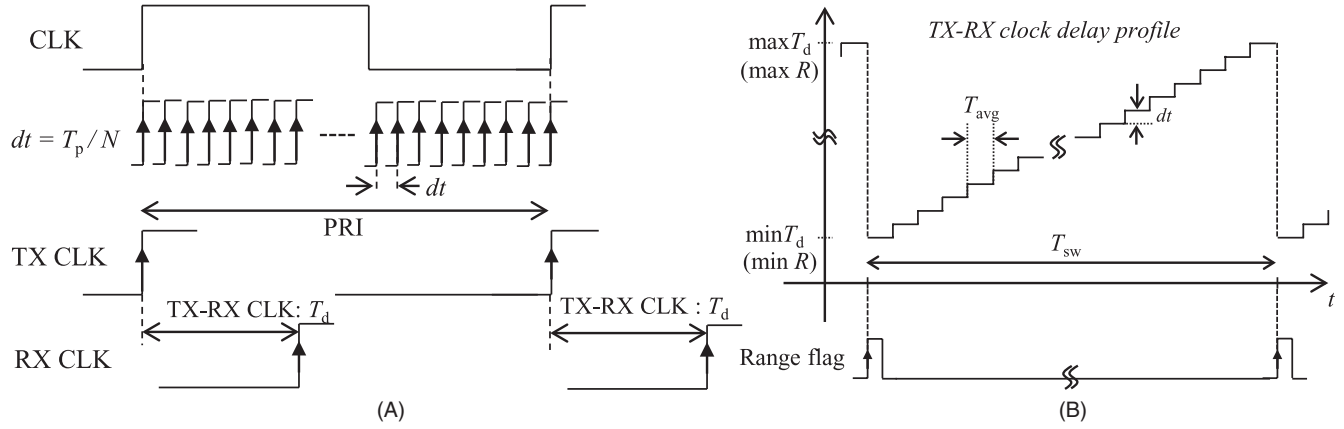

FIGURE 2 Timing diagram of the radar (A) clock signal, timing resolution(t), TX and RX clocks, and (B) TX–RX delay profile

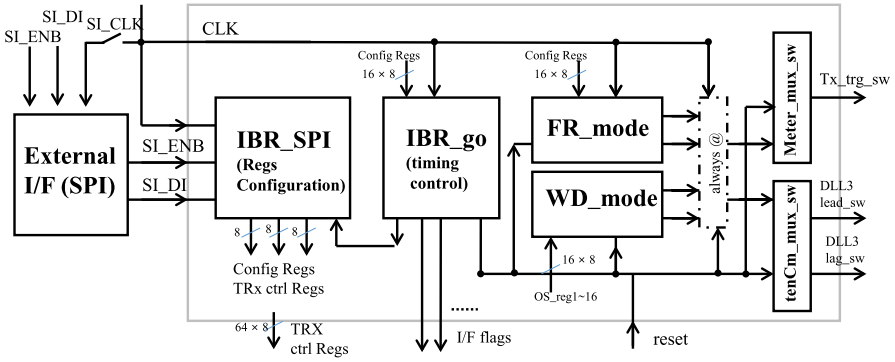

FIGURE 3 Embedded radar control logic for the through-the-wall radar (TTWR) [Colour figure can be viewed at wileyonlinelibrary.com]

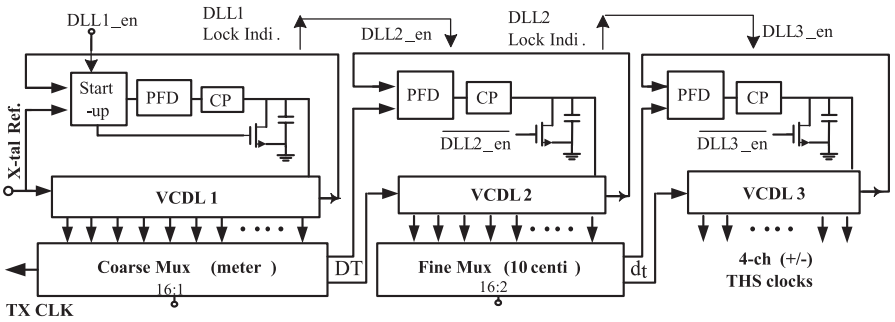

FIGURE 4 Clock generator block diagram

RX clocks are used. Figure 2B shows the TX–RX delay (T_d) profile for the range sweep between R_{min} to R_{max}. The profile is reconfigurable for a specific user environment.

For example, with a PRI of 100 ns (15-m range: $0{:}5c \times$ PRI), a resolution of a 100 ps delay results in 1k samples (100 ns/100 ps) and it takes 100 μs (1k × 100 ns). By applying repetitive samplings for each range, the recovery time will increase to 10 ms (100 μs × 100). Therefore, the time-expansion radar allows us to observe a 100 ns range within the 10 ms timeframe. Furthermore, repetitive reception at the same point range improves the SNR. Based on the weak law of large numbers [15], reception approaches signal values (ie, mean), while noise (ie, variance) drops proportionally with respect to the number of samples.

2.3 | Transceiver architecture

Figure 1 depicts the block diagram of the proposed through-wall radar system. Being restricted by the small-form factor as well as performances, a radar SoC with reconfigurability is optimal. To achieve this, the control logic is embedded as found in Figure 1B. An external processor can control the radar operation and perform the signal processing. The external processor can easily handle generic inputs/outputs (IOs), such as the displays and switches. The radar operates in real time. Continuous receiving/digitizing echo pulse and processing operations used to obtain target information are conducted. Details are discussed in the following section.

Clock-synchronized RX and TX operations are performed. The clock generator produces all the necessary clock signals, and the control logic adjusts the clock delay and sets the delay profile. The detection range is set by choosing TX–RX delay, T_d, and coherent reception is achieved by adjusting, T_{avg}, as seen in Figure 2. The controller also contains 64 registers that can tune the transceiver characteristics, such as the receiver gain allocation, impulse width, and the center frequency. The radar link (1) indicates that a sensitivity better than ~ −70 dBm is required for a beyond-the-wall human target with a height of 4 m (RCS of 0 dBsm, wall loss of 30 dB). A coherent detection gain of 20 dB is assumed. The gain is distributed in the RX chain as follows: adjustable gain of 5 dB–35 dB for the low-noise front-end stage, >40 dB of dynamic range at the final stage of the operational transamplifier (OTA). The bandwidth for the RX sampler (THS) is targeted and is >5 GHz. A transmitter bandwidth of 3 GHz–5 GHz with an adjustable pulse width is aimed to mitigate possible process-voltage-temperature (PVT) variations.

2.4 | Hand-held prototype

The prototype TTWR is shown in Figure 8. The prototype system displays the real-time target information at the rear display unit. The radar SoC interfaces with an external processor. A commercially available single-board computer (SBC) is used, and a 5 V rechargeable battery powers the system. The SBC is based on the ARM™A8 processor featuring 1 GHz clock speed and 2000 MIPS. The SBC configures the radar SoC and collects the reception data through an analog-to-digital converter (ADC). Real-time operation is performed. The SBC maintains the routine of completing the

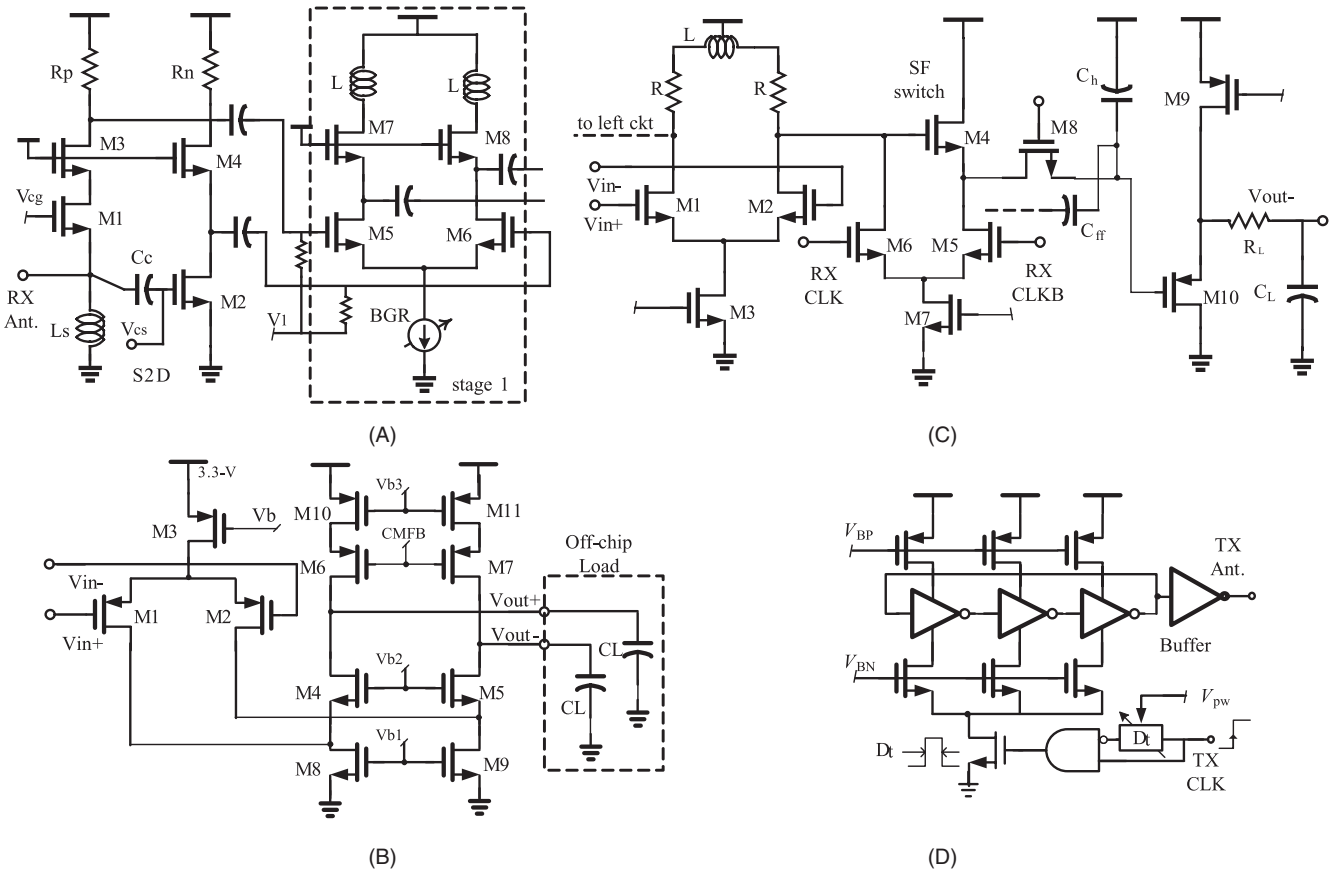

FIGURE 5 Transceiver circuit block diagram: (A) A single stage of the three-stage, front-end, low-noise amplifier (LNA) is shown, (B) wideband sampler (half the circuit is shown), (C) back-end gain stage, and (D) spectrum adjustable transmitter

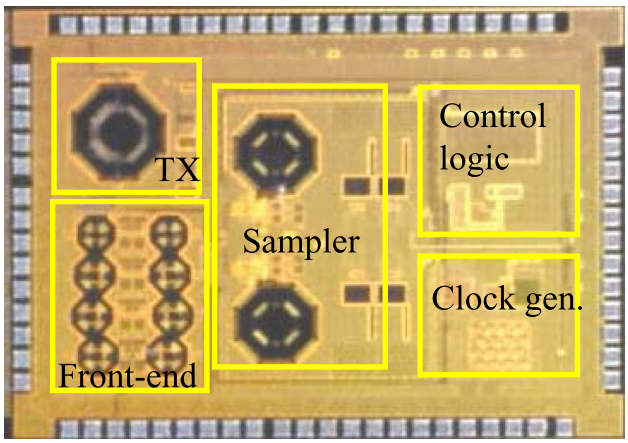

FIGURE 6 Chip micro-phot [Colour figure can be viewed at wileyonlinelibrary.com]

TABLE 3 Test conditions and results [16, 17]

Conditions[a]	Subjects	Results[b]
Smoke	Walking man, corridor	>10 m
Wall1	Walking man, room	>3.5 m
Wall2	Walking man, room	>3.5 m
Wall3	Walking man, room	>3.5 m
Debris[c]	Torso movements, collapse	at 2 m

[a]Conditions [16], wall1 (ALC block), wall2 (board wall), wall3 (tile wall).
[b]detection probability in [16] from multiple experiments (> 20): > 95%.
[c]Tested at disaster research infra at Young-il Bay, Pohang [18].

data process before new data become available. The operation flow chart is shown in Figure 11.

Wideband antennas (3 GHz-5 GHz) shown in Figure 8 are used in the TTWR. The antenna has a gain of ~9 dBi and the return loss, $S11$, is less than −10 dB. Four-patch design with back-plane reflector is adopted for high directivity. The radar has a gun-shaped exterior for intuitive operation. The radar operates by point-and-shoot with a trigger. A readily available 5-V rechargeable battery powers the system. The system can operate for more than an hour continually.

3 | CIRCUIT IMPLEMENTATION

This section describes a circuit implementation of the proposed radar SoC. The supported radar operations include the variable detection range, SNR enhancement, and transceiver adaptation. The embedded control logic and its

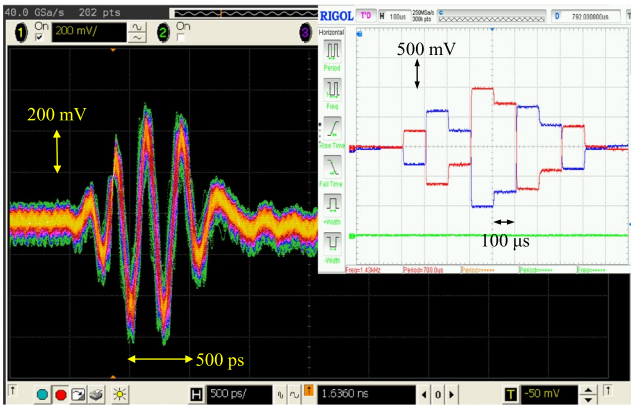

FIGURE 7 Transmitter impulse waveform and its recovered waveform from the receiver. Transmitter-to-receiver loop-back test with an attenuator was conducted

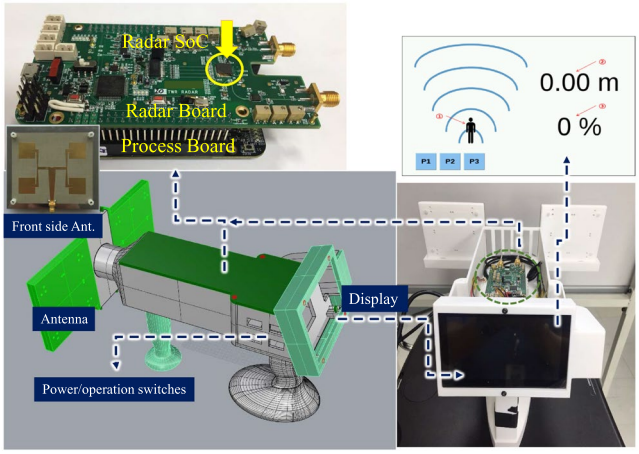

FIGURE 8 Through-the-wall radar prototype system used in the experiments

interface with the radar clock generator are stressed. The impulse transmitter and the wideband sampling receiver are explained.

3.1 | Embedded radar controller

As discussed, to overcome the harsh invisible conditions, the radar operates based on the clock signals that allow reconfigurable operations. The logic is implemented with a hardware description language (HDL), and is integrated in the radar SoC to achieve detection range selection, SNR enhancement for wall penetration, and transmitter and receiver mode settings. The controller interfaces with an external SBC with serial peripheral interface (SPI) with which the radar operation is set. The radar detection range is controlled by altering the TX-RX time delay, as discussed in Section 2.2. It is possible to selectively include (or exclude) the range of interest. The range exclusion affected by the wall, or an inclusion for the interest range is possible. The range selection, that is, the full-range (FR)/window (WD) mode shown in Figure 3, can flexibly adjust the TX-RX delay based on the selection of the switches in the clock generator, as discussed in the next section.

Radar transceiver modes are adjustable by setting the reference biases in the transceiver. Receiver sensitivity and linearity are controlled by selecting the gain distribution in the receiver stages. Tradeoffs between sensitivity and linearity can be achieved in different conditions. Increased sensitivity in smoke conditions results in the longer range, while through-wall operations require linearity and SNR enhancement set with increased, T_{avg} values. The impulse shape of the transmitter—pulse width and frequency—can be controlled, as discussed in the next Section 3.3.

3.2 | Clock generator

The radar operates with clock signals in a synchronous manner. From a 10 MHz reference clock signal, the clock generator that adopts delay locked loop (DLL) defines fine delays based on the delay in controllable delay lines [7]. Figure 4 shows the block diagram of the clock generator. Fine delays of ~100 ps (~1k phases) are available formulated in the form of δt in Figure 2A. Therefore, the range resolution is 1.5 cm. A TX-RX delay (ie, detection range) is selected by choosing multiplex (Mux) switches in the DLL. From the coarse Mux, one can select the time delay of a meter resolution whereas a centimeter resolution is attained from the fine Mux. By using a multistage architecture, the area and power efficiency is achieved. By changing the ~1k delays selection into the combination of the coarse and fine Mux switches, ease of control is also achieved. To ensure the lock of DLL with the reference clock, the DLL lock indicator flags are used.

3.3 | Impulse radio transceiver

While interfacing an RX antenna, a front-end low-noise amplifier (LNA) converts the single-ended impulse signals into differential ones. Subsequently, cascaded three-stage differential pairs observed in Figure 5A further amplify the signal. To obtain a wide bandwidth, the gains at the peak-frequencies are staggered at each stage. The programmable gain can be set for the optimal reception of the impulse. The simulation results show that the maximum gain of 40 dB at 4 GHz and the bandwidth is >1 GHz. As mentioned in Section 2, a sampler-based receiver directly samples the received echo pulses using a wideband sampler. With the clock scheme, the sampling also allows the additive reception of the echo signals. The RX clock signals drive the wideband sampler, as shown in Figure 5B to sample the amplified impulse from the LNA. The source

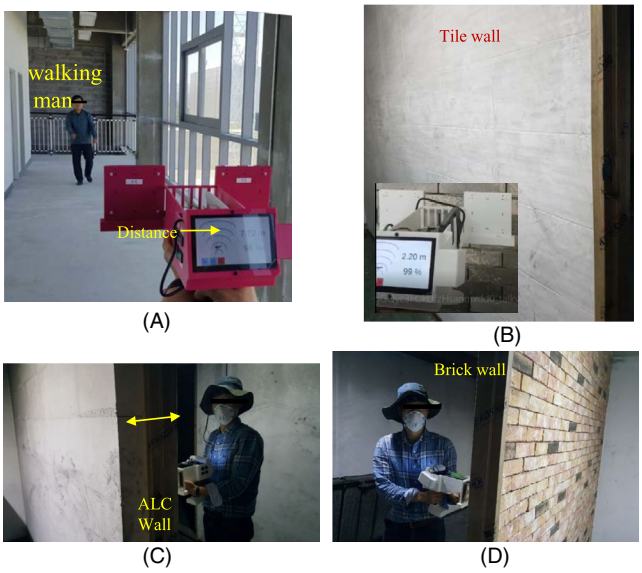

FIGURE 9 Exemplary in-door experimental environments: (A) open corridor, (B) tile wall, (C) autoclaved lightweight aerated concrete (ALC) wall, and (D) brick wall [Colour figure can be viewed at wileyonlinelibrary.com]

follower switch is adopted to attain a wide bandwidth [7]. The final stage of the RX interfaces with external components, typically with an ADC on board. To maintain the desired amplitude and common-mode level for the received impulse signal, an operational transconductance amplifier (OTA) depicted in Figure 5C is utilized. Capacitor loads on board for the OTA act as a filter that suppresses on-board clock noise. The radar system consists of multiple boards. Thus, on-board clock noise suppression is important.

The transmitter radiates impulses that occupies 3 GHZ-5 GHz spectrum at the rising edges of the TX clocks by utilizing a triggered oscillator. The circuit diagram of the triggered oscillator is shown in Figure 5D. The TX clock signal initiates the oscillation of the starved ring oscillator for variable time (ΔT). The delay of the ring oscillator can be set. As a result, the variable pulse width and center frequencies are achieved [7]. Two low drop out (LDO) circuits are used so that (a) the TX prevents TX pulses from coupling to the supply voltage and (b) the RX maintains a clean supply voltage for the front-end circuits. Digitally controlled small-sized, 8-bit, R-2R DACs are used for bias control for the SoC (Figure 6).

4 | MEASURED RESULTS AND DISCUSSIONS

The prototype radar is evaluated at different scenarios according to the test standards for human detection at disaster scenes [6–18]. This section describes test methods, environments, and the measured results of the prototype radar.

4.1 | Measurement environments

Disaster scenes where the prototype radar is used cannot be easily reproduced in a laboratory environment. The performances, however, need to be confirmed at the disaster scenes. The specialized test site has been constructed for disaster response research studies [18]. The prototype radar was tested onsite. the limited visibility conditions due to aerosol particles, beyond-wall detection (various materials), and collapse debris are quantified. The test standards for the human-life detection radars are established. Test environments, test methods, detection range, and human poses are defined [16]. The measured results are summarized in Table 3.

4.2 | Measured results

Before building the prototype TTWR, the radar SoC is tested in a separated board to confirm the functionalities. With a direct TX-to-RX through connection (proper attenuators), the controllability and radar operation modes for different environments are checked. Figure 7 presents the measured transmit pulse from the antenna port. The pulse width of ~1 ns and the amplitude of 1 V_{pp} are shown. The center frequency of the impulses is ~4 GHz. The variable bandwidth (sub-ns to tens ns) is attained by setting V_{PW}, as shown in Figure 5D. The recovered pulse from the RX is shown in the inset. The clock was set to sweep the range after 1000 repetitive reception cycles (see Figure 2). Given that a PRI of 100 ns is used, 100 μs (1000×100 n) of T_{avg} is observed. The measured power dissipation of the radar SoC is less than 120 mW which is a fraction of the prototype system dissipation (Table 4).

The prototype TTWR shown in Figure 8 displays real-time target information on the screen Figure 9; the radar is also able to keep raw data on the storage device for the post analysis. Detection for walking man is conducted in an open corridor with visible distance <2 m, as defined in [17]. Figure 10A Shows measured data of a single radar frame, that is, the range and the target amplitude response. The radar updates the frame every 78 ms after five frame collections and their preprocessing. To get the frame data, the clock signals are generated according to the predefined TX-RX delay profile (see Figure 2B) and drive the radar transceiver. The range point of 650 that corresponds to ~9.8 m is set for the experiments. The preprocessing includes a moving target indication (MTI) filter which subtracts the stationary background noise from the current frame. The previous k frames are weighted optimally for the best detection in each scenario as follows,

$$f_{\mathrm{MTI}}[n] = f[n] - kTOTO \sum w_k f[n-k].$$

Figure 10B shows the range decision points (ie, target location) at each frame. The target location displayed on the

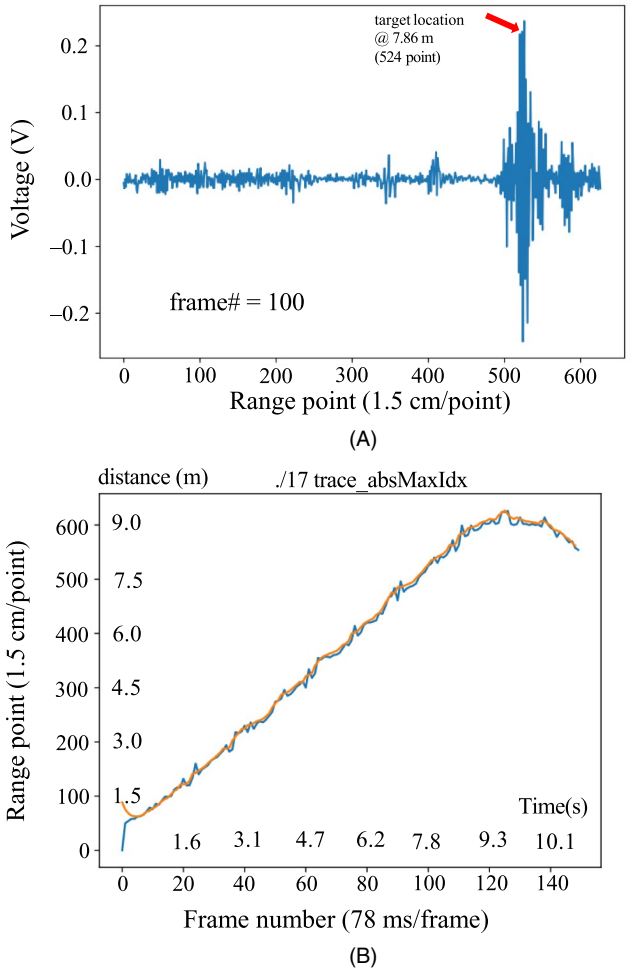

FIGURE 10 Experimental data for a man walking in a corridor: (A) A-scan raw data and (B) target location at the frame [Colour figure can be viewed at wileyonlinelibrary.com]

screen of the prototype radar is replotted with time. The blue (fluctuated) line shows the raw point range following the threshold target decision. The smooth (orange) line corresponds to the estimation based on the Kalman filter. Large jumps at the target range from the previous locations will have diminishing effects for the update of the newly estimated target location, thus yielding a low-pass response. The flow chart of the radar is presented in Figure 11.

The TTWR was tested under the collapse debris in [18] with several materials. Figure 12 shows the experiment scene, whereby debris is mostly contributed from concrete walls and some from wood boards. The pile thickness is greater than 0.5 m. With restricted motion within 1 m, the radar reception is mainly attributed to the torso and upper body movements of the target. The bottom part of Figure 12 shows the response from thick debris and periodical movements from the target.

Figure 13 shows the experimental results for the through-wall detection. A walking human target beyond autoclaved

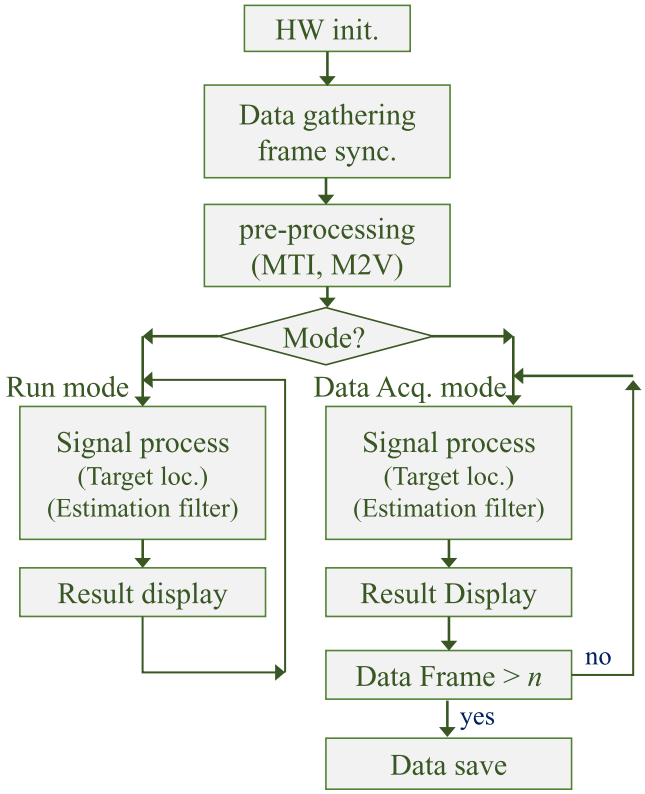

FIGURE 11 Prototype radar operation flow diagram [Colour figure can be viewed at wileyonlinelibrary.com]

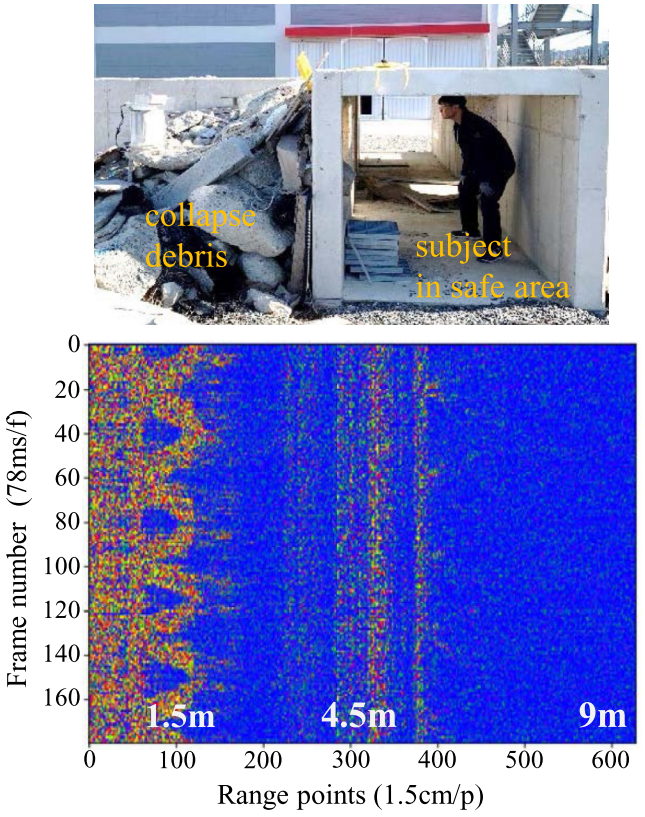

FIGURE 12 Collapse debris experiment and results [Colour figure can be viewed at wileyonlinelibrary.com]

TABLE 4 Radar transceiver ICs and through-wall radar comparison

Features	This work	[2]	[8]	[9]	[10]
DUT (Weight)	Prototype system (0.9 kg)	Commercial product (7.5 kg)	Test board (-)	Test board (-)	Test board (-)
Transceiver	Radar SoC	Discrete module	Radar SoC	Radar SoC	Radar SoC
Integration (Tech.)	TX/RX/Logic (130n)	Discrete ICs	TX/RX (130n)	TX/RX/ADC (55n)	TX/RX (130n)
Target	Through-wall	Through-wall	Walking	Breathing	Movements (2.5 mm)
Operation[a]	UWB	UWB	UWB	UWB	Impulse
Frequency band (GHz)	3–5	0.4 ± 30%	0.8–5	7.29 ± 1.4	0.5–1
R_{max},ΔR (m, cm)	15, 1.5	12, 7.5	15, 0.75	9, –	–, 0.25
Precision (mm, ps)	15	NA	N/A	4.2[b]	2.5
Power dissipation (mW)	115	NA	695	118	30
Chip area (mm^2)	3.1	NA	11.9	8.6	1

[a]UWB band definition FCC, ITR-R (ITU-R SM.1755-0).

[b]Sampling rate 23.328 GS/s.

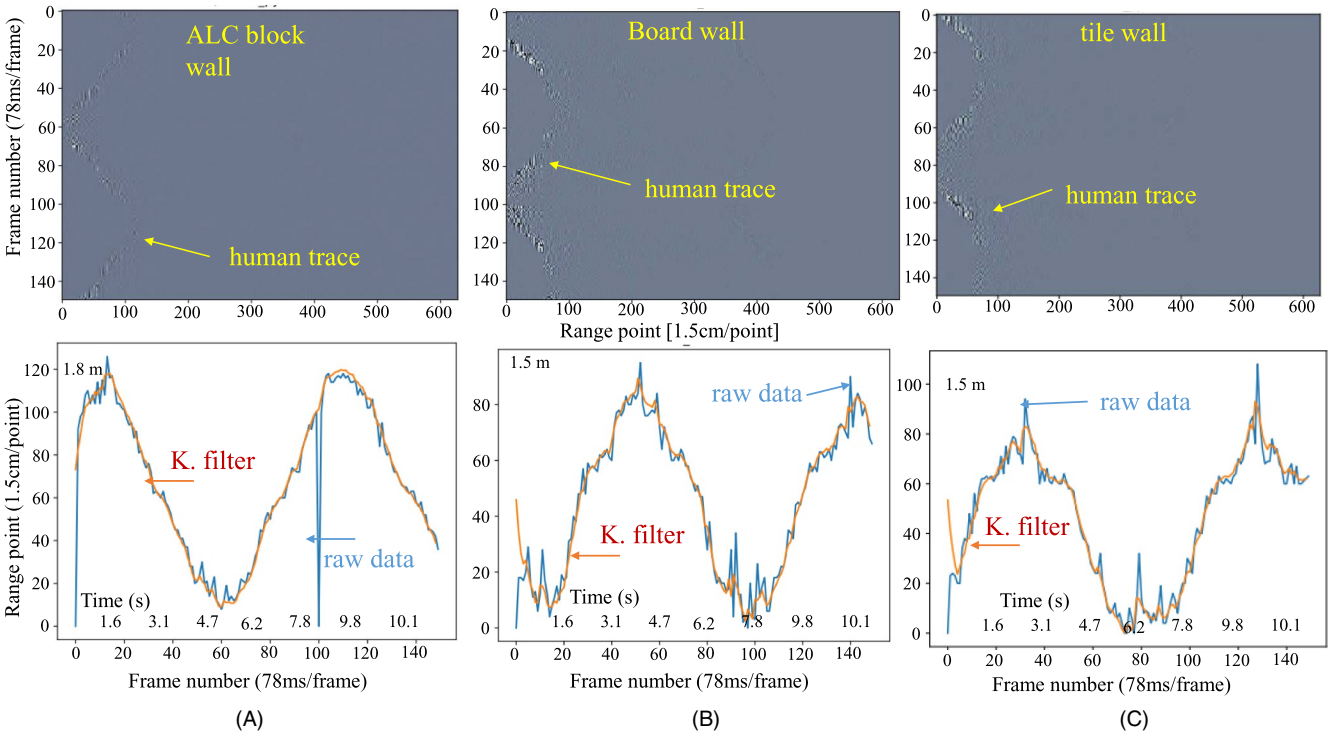

FIGURE 13 Through-wall measurements: (A) Autoclaved lightweight concrete (ALC) block wall, (B) plaster board wall, and (C) tile wall [Colour figure can be viewed at wileyonlinelibrary.com]

lightweight concrete (ALC) block wall (thickness 20 cm) is measured and the results are shown in Figure 13A. The upper figures show b-scan images, that is, aggregations of a-scan data in two-dimensions (2D) (an example of an a-scan is shown in Figure 10A) wherein the target location (range in *x*-axis) vs time (frame number in *y*-axis) is shown. In the bottom figure, the target location point (*y*-axis) is plotted at each frame (*x*-axis). As observed, the estimation filter corrects some of the false target locations from the raw data. Figure 13B and C correspond to the different walls (plaster board and tiled wall, respectively). Note that the limited range in the test data is attributed to the room size.

A detection range greater than 3.5 m is measured for the walking man beyond the ALC concrete wall with a thickness of 20 cm.

5 | CONCLUSIONS

Through-wall radars can enhance efficiency in rescue operations and particularly in disaster scenes with limited visibility owing to smoke, walls, and collapse debris. To overcome increased losses in the radar link, and to maintain small-form factors, an SoC radar for the TTWR is proposed. Additive reception based on the coherent clock and reconfigurability fulfills the demands for TTWRs. The SNR is enhanced with clock-based coherent reception. Reconfigurability of the radar reception is critical and optimal radar settings are different at the various conditions. Embedded radar logic interfacing through SPI sets the radar operation mode and transceiver conditions.

The clock-based radar transceiver architecture is implemented. The clock generator (100 ps resolution) was tightly interfaced with the radar logic and provided all the necessary clock signals for the radar. The clocked impulse transmitter and the wideband sampling receiver were also optimized.

Measurement conditions and scenarios were proposed, and test standards for a human-life detection radar sensor were established [16,17]. The specialized facility for disaster response has been constructed. The prototype radar was measured with the established test standards. The prototype operated in real time and displayed the detection results on screen by responding to the user trigger input. In a nonblocking scene (smoke), a detection range greater than 10 m was measured. For beyond-wall human-detection applications, a detection range greater than 3.5 m was achieved.

ACKNOWLEDGMENTS

The authors are grateful to Professor Seo at SKKU for the antenna design and implementation (KEIT 10067194). This work was partially supported by the "Industrial Technology Innovation Program" Grant 10067194 and "ETRI support program" 2019-0-00006.

ORCID

Piljae Park https://orcid.org/0000-0002-0655-531X

REFERENCES

1. Statistical year book 2019. Section 3. Korean National Fire Agency. http://www.nfa.go.kr/nfa/.
2. N. Scmcykin, A. Dudnik, and V. Monahov, *Low frequency through-wall radar-detector*, in Proc. Int. Conf. Ground Penetrating Radar(Brussels, Belgium), 2014, pp. 819-822.
3. G. Inanan et al., *Handheld Ultra-Wideband Through-Wall Radar*, in Proc. Seminar Detection Syst. Architectures Technol. (Algiers, Algeria), 2017, pp. 1-6.
4. Camero-tech, XAVER systems. https://www.camero-tech.com/xaver-products/xaver-100/.
5. Camero-tech, XAVER systems, Cambridge Consultants. https://www.cambridgeconsultants.com/.
6. H. Burchett, *Advances in through wall radar for search, rescue and security applications*, in Proc. IET Conf. Crime Security (London, UK), pp. 511–525.
7. P. Park, et al., *A centimeter resolution, 10 m range CMOS impulse radio radar for human motion monitoring*, IEEE J. Solid-State Circuits **49** (2014), 1125–1134.
8. T. Chu et al., *A short-range UWB impulse-radio CMOS sensor for human feature detection*, in Proc. IEEE Int. Solid-State Circuits Conf. (San Francisco, CA, USA), Feb. 2011, pp. 294-296.
9. N. Andersen et al., *A 118-mW pulse-based radar SoC in 55-nm CMOS for non-contact human vital signs detection*, IEEE J. Solid-State Circuits **52** (2017), 3421–3433.
10. P. Park, and S. Kim, *A continuous sweep-clock-based time-expansion impulse-radio radar*, IEEE Trans Circuits Syst. I Regul. Pap. **65** (2018), 3049–3059.
11. S. Kim et al., *A Subthreshold CMOS RF front-end design for low-power band-III T-DMB/DAB receivers*, ETRI J. **33** (2011), 969–972.
12. M. Khurram et al., *A 35 GHz current-reuse* g_m*-boosted CG LNA for Ultrawideband in 130 nm CMOS*, IEEE Trans.Very Large Scale Integr. (VLSI) Syst.,, **20** (2012), no. (3), 400–409.
13. F. D. David Jr, and C Nicholas, *Currie Microwave and millimeter-wave systems for wall penetration*, Proc. SPIE 3375, Targets and Backgrounds: Characterization and Representation IV, July 1998, pp. 269–279.
14. L. Yishan et al., *Analysis and measurment of wall penetration loss as a function of incident angle*, in Proc. Int. Workshop Electromagnetics (London, UK), 2017, pp. 124–125.
15. D. Bertsekas and J. Tsitsiklis, *Introduction to Probability. 2nd ed*, Athena Scientific, 2008, p. 269.
16. KROS standard 1136:2018, *Performance evaluation method for human-life detection for disaster response robots*, Korean Industrial Standards, Smart robot standard forum, SC-5 section, http://www.koros.or.kr/.
17. KIRO standard 2019, *Performance evaluation methods for a human-life detection sensor in disaster environments*, http://drc.re.kr/research/test_certify.php.
18. Disater response robot field test facility, Pohang, Young-il bay, http://drc.re.kr/research/facility.php.

AUTHOR BIOGRAPHIES

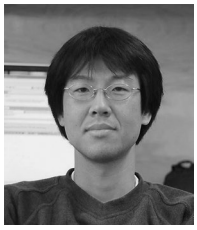

Piljae Park (Senior member of *IEEE*) received his PhD degree in Electrical and Computer Engineering from University of California, Santa Barbara in 2009. During his PhD study he explored wireless circuitry and transceivers for on-wafer wireless testing. His *IEEE 2009 RFIC Conference* paper was in the final list of the best student paper competition. Since 2000, he has been with SoC Research Laboratory at Electronics and Telecommunications Research Institute (ETRI), Daejeon, South Korea, where he is currently conducting research on integrated radar systems. His patent portfolio covers on-chip radar architectures for near-range, high-resolution applications. His patents are pivotal for high-performance implementation and mass production. Some of recent works have been successfully commercialized through the technology transfer program at ETRI. His research interests include radiofrequency (RF)/analog and mixed-mode circuit design for sensor applications.

Sungdo Kim received his ME degree from the Information and Communications University (ICU), Daejeon, in 2002 and his PhD degree from Chungnam National University, Daejeon, Korea, in 2010, all in Electronics Engineering. Since 1989, he has been with the Electronics and Telecommunications Research Institute (ETRI) where he has been working on CMOS RF/Analog circuits and RF front-end architectures. He was the co-recipient of the presidential award in the 9th Semiconductor Design Competition for his digital multimedia broadcasting (DMB) SoC. His research interests are in CMOS RF/Analog circuit design and high-speed mixed-signal integrated circuit (IC) design for wireless communications and radar sensors.

Bontae Koo received his MS degree in Electrical Engineering from Korea University, Seoul, Republic of Korea, in 1991. In 1991, he was at the System Semiconductor Division of Hyundai Electronics, Ichon, Korea. where he was involved in the chip design of video codec and DVB modem. From 1993 to 1995, he was at HEA, San Jose, USA, where he designed the MPEG2 video codec chip. From 1996 to 1997, he was at TVCOM, Sandiago, USA, and developed the design of the DVB modem chip. In 1998, he joined Dongbu Electronics, as a team leader with the system semiconductor Lab, and he focused on the methodology of semiconductor chip design. In 1999, he joined the application SoC team, ETRI, where he was a team leader. His research activities included the chip design of MPEG4 video, T-DMB receiver, LTE femtocell modem and DSP processor. In 2016, he joined RF research group in ETRI, where he is currently a project leader. His research activities focused on millimeter-wave AI radars.